PAPER

First observation on emergence of strong room-temperature ferroelectricity and multiferroicity in 2D-Ti$_3$C$_2$T$_x$ free-standing MXene film†

Rabia Tahir,[a] Syedah Afsheen Zahra,[a] Usman Naeem,[a] Deji Akinwande[b] and Syed Rizwan [ID] *[a]

Two-dimensional (2D) multiferroics are key candidate materials towards advancement of smart technology. Here, we employed a simple synthesis approach to address the long-awaited dream of developing ferroelectric and multiferroic 2D materials, especially in the new class of materials called MXenes. The etched Ti$_3$C$_2$T$_x$ MXene was first synthesized after HF-treatment followed by a delamination process for successful synthesis of free-standing Ti$_3$C$_2$T$_x$ film. The free-standing film was then exposed to air at room-temperature and heated at different temperatures to form a TiO$_2$ layer derived from the Ti$_3$C$_2$T$_x$ MXene itself. The ferroelectric measurement showed a clear polarization hysteresis loop at room-temperature. Also, due to the reported ferromagnetic behavior of Ti$_3$C$_2$T$_x$ MXene, our composite could show multiferroic properties at room-temperature. The magnetoelectric coupling test was also performed that showed a clear, switchable spontaneous polarization under applied magnetic field. TiO$_2$ is reported to be an incipient ferroelectric that assumes a ferroelectric phase in composite form. The structural and morphological analysis confirmed successful synthesis of free-standing film and the Raman spectroscopy revealed the formation of different phases of TiO$_2$ and the observed ferroelectricity could be due to structural deformation as a result of the formation of this new phase. The measured value of remanent polarization is 0.5 μC cm^{-2}. This is the first report on the existence of a ferroelectric phase and multiferroic coupling in 2D free-standing MXene film at room-temperature which opens-up the possibility of 2D material-based electric and magnetic data storage applications at room-temperature.

Introduction

Due to interesting physical and electronic properties for diverse applications, designing two-dimensional (2D) multiferroic materials has been a dream for researchers.[1–3] In multiferroics, two or more ferroic phases are coupled through piezoelectric, magnetoelastic or magnetoelectric (ME) interaction in such a way that one ferroic phase is tuned and controlled by another upon external perturbation and *vice versa*. In ME interaction, the magnetic field (or electric field) can tune the spontaneous polarization (or magnetization) in a single material or composite thus, providing a unique opportunity to develop smart sensors, non-volatile memories, small electronic devices, *etc.* that might lead to the miniaturization of electronic

gadgets.[4] There are numerous reports on the existence of multiferroic phases in bulk materials however, the miniaturization of electronic devices requires developing multiferroicity in materials in low-dimensions.[5] One possible solution is to develop 2D materials that are smaller in size and easy to synthesize however to the best of our knowledge, experimentally the existence of ferroelectricity in MXenes, and two ferroic phases in 2D materials has not been realized yet. Experimental and theoretical reports on 2D ferroelectrics and multiferroics are listed in Tables 1 and 2.

Ferroelectric materials possess an inherent switchable spontaneous polarization that can be tuned using an external electric field.[22] A very few 2D materials have been predicted to be ferroelectric and the experimental reports on 2D ferroelectrics are even rare. Molybdenum di-sulfide (MoS$_2$), a candidate 2D material from transition metal chalcogenides (TMCs) family, is reported to reveal ferroelectricity under high pressure.[23] The authors created bi-domain polarization under mechanical stress leading to polar distortion in symmetric monolayers generating ferroelectric-type distortion. The binary oxides such as TiO$_2$ are also important material candidates owing to potential applications in dielectric, photocatalysis, *etc.*[24] TiO$_2$ is also known to be an incipient ferroelectric material that shows

[a]*Physics Characterization and Simulations Lab (PCSL), Department of Physics, School of Natural Sciences, National University of Sciences and Technology (NUST), H-12 Islamabad, Pakistan. E-mail: syedrizwan@sns.nust.edu.pk; syedrizwanh83@gmail.com*

[b]*Microelectronics Research Center, The University of Texas at Austin, Austin, TX 78758, USA*

† Electronic supplementary information (ESI) available. See https://doi.org/10.1039/d2ra04428e

Table 1 Experimental and theoretical reports on 2D ferroelectrics

S. No.	Name	MXenes	2D Materials other than MXenes	Experimental/theoretical	Ref.
1	Sc_2CO_2	✓		Theoretical	6
2	Nb_2NF_2	✓		Theoretical	7
3	$Ti_3C_2T_x$	✓		**Experimental**	**This work**
4	SnS		✓	Experimental	8
5	SnSe		✓	Experimental	9
6	d1T-$MoTe_2$		✓	Experimental	10
7	WTe_2		✓	Experimental	11
8	BA_2PbCl_4		✓	Experimental	12
9	$2H$ α-In_2Se_3		✓	Experimental	13
10	β'-In_2Se_3		✓	Experimental	14
11	In_2Se_3		✓	Experimental	15
12	α-In_2Se_3		✓	Experimental	16
13	SnTe		✓	Experimental	17
14	$CnInP_2S_6$		✓	Experimental	18

ferroelectricity in proximity in its composite form.[25] Y. Yu *et al.* reported successful generation of local broken symmetry causing observation of ferroelectricity in TiO_2.[26] Theoretical predictions also suggest that under high mechanical or uniaxial strain, TiO_2 can reveal ferroelectricity at room-temperature however, this is still to be observed experimentally.[25,27]

Transition metal carbides, known as MXenes with general chemical formula $M_{n+1}X_nT_x$, (where, M = Sc, Ti, V, Cr, Zr, Nb, Mo, Hf, Ta and X = C, N while n = 1,2,3), are emerging 2D materials owing to their rich physical and chemical properties suitable for vast avenue of applications such as in transparent conductors,[28,29] supercapacitors,[30–32] transistors,[33–35] electromagnetic shielding,[36] photocatalysis,[37] *etc.* Sunaina *et al.* reported presence of ferromagnetism in Ti_3C_2Tx MXene at room-temperature which was further enhanced upon doping with a magnetic element.[38] Similar studies were also reported in this compound suggesting that $Ti_3C_2T_x$ is a good material candidate among MXene family that might be suitable for spintronic applications.[39] Another report on Nb_2C MXene reported the diamagnetic-type superconductivity with relatively higher transition temperature of 12.5 K.[40] These reports clearly reveal the hidden potential of MXene in magnetic data storage devices, magnetic sensors, *etc.* Moreover, J. X. Low reported synthesis of Ti_3C_2-MXene/TiO_2 composite formed by calcination at different temperatures which provides a scheme way to prepare Ti_3C_2-MXene composites useful for various applications.[41]

In this report, we have employed a simple and cost-effective strategy to develop ferroelectricity in free-standing $Ti_3C_2T_x$

MXene film. Since TiO_2 is reported to be an incipient ferroelectric, we assumed the emergence of ferroelectricity in MXene-derived TiO_2/$Ti_3C_2T_x$ free-standing film. To prepare this composite with an optimal TiO_2 ratio in the composite, MXene was air-exposed at room-temperature and was heated at higher temperatures. The presence of TiO_2 was confirmed using Raman spectroscopy technique. The ferroelectric testing performed at room-temperature clearly showed the ferroelectric hysteresis. Further, the magnetic testing of the free-standing composite film confirmed the existence of ferromagnetism in the compound thus, paving the way to create the multiferroicity in prepared composite. To confirm this assumption, magneto-electric testing was also performed that showed a clear magnetic-field control of spontaneous polarization suggesting it to be a very good multiferroic 2D material. Our results, presented here, are the first report on existence of ferroelectricity and multiferroicity induced in MXene-derived TiO_2/$Ti_3C_2T_x$ free-standing film at room-temperature prepared using a simple synthesis approach which will open new avenues for 2D MXene multiferroics to be employed in electric and magnetic data storage applications.

Experimentation

Synthesis of $Ti_3C_2T_x$ free-standing MXene film

$Ti_3C_2T_x$ MXene was prepared by selectively eliminating 'Al' from the Ti_3AlC_2 MAX phase. The commercial grade Ti_3AlC_2 MAX powder was used. In a typical process, 1.0 g of sieved Ti_3AlC_2

Table 2 Experimental and theoretical reports on 2D multiferroics

S. No.	Name	MXenes	2D Materials other than MXenes	Experimental/theoretical	Ref.
1	$Hf_2VC_2F_2$	✓		Theoretical	19
2	Ti_3C_2	✓		**Experimental**	**This work**
3	SnS		✓	Theoretical	20
4	SnSe		✓	Theoretical	20
5	GeS		✓	Theoretical	20
6	GeSe		✓	Theoretical	20
7	NiI_2		✓	Theoretical	21

MAX phase is immersed in the solution containing Hydrofluoric acid (≥48 wt%, 1 ml HF) (Sigma Aldrich), deionized water (3 ml DI) and hydrochloric acid (37 wt%, (12 M) 6 ml HCl) in a ratio of 1 : 3 : 6 (volume ratio) under constant stirring at 450 rpm for 24 hours at 35 °C. The sieved Ti_3AlC_2 powder was steadily added in increments over 5–8 min in a Teflon-lined reaction vessel before it was sealed. Once done, it was rinsed with DI multiple times. After each cycle, the supernatant was discarded to eliminate any undesirable adsorbed ions. The sediment was dispersed in DI until the pH reached 7. The etched powder was then collected by filtration and dried overnight at room temperature.

Subsequently, the multilayer (ML)-$Ti_3C_2T_x$ MXene was delaminated using LiCl (lithium chloride, 99%).[42] The ML-MXene powder was dispersed in 20 ml of DI, 1 g of LiCl was then added, and the mixture was shaken hard for 8–10 min. The solution was then kept under constant stirring at 300 rpm for 24 h. The resulting intercalated dispersion was centrifuged with DI at 3500 rpm for 5 min; the centrifugation was performed repeatedly until a stable colloidal MXene solution was achieved. Following separation, additional DI was added to the sediment, which was then re-dispersed and centrifuged again. This was repeated until the supernatant produced was dilute. The resulting wet sediment formed a clay-like paste which was centrifuged for 30 min at 3500 rpm to ensure that no ML powder remained. The supernatant MXene solution that remained stable after extended centrifugation was vacuum filtered *via* Celguard membranes, which were then used to form free-standing films (Fig. 1). The thickness of synthesized $Ti_3C_2T_x$ free-standing MXene film was measured by using micro screw gauge which is ~21 μm. Generally, centrosymmetry is broken when 2D material's surfaces are asymmetrically functionalizes that results in out of plane polarization. So, the 2D layered structure of MXene is favorable for the induction of ferroelectricity if the desired functional groups *i.e.* O, OH, S, Cl or F are attached on the surface of MXene that play a big role to tune their electronic properties. So, heat treatment is done for the oxidation of $Ti_3C_2T_x$ MXene which results in formation of TiO_2 which possibly give rise to non-centrosymmetric structure that probably induced the coexistence of in-plane and out of plane electric polarization under the application of external field.[43] For oxidation, it was reported that $Ti_3C_2T_x$ gets optimum oxidation by heat treatment.[41] So, the synthesized $Ti_3C_2T_x$ MXene film was heat-treated for 2 hours at 100 °C (namely HT@100 °C), 150 °C (namely HT@150 °C), and 300 °C (namely HT@300 °C) under an ambient environment.

Ferroelectric/multiferroic measurement setup

For ferroelectric/multiferroic testing, the precision tester from Radiant Technologies Inc. was used. The sample stage for mounting the sample is shown in Fig. 2(a). The prepared $Ti_3C_2T_x$ free-standing MXene film was mounted on sample stage has dimensions of about 0.2 cm × 0.4 cm having thickness ~21 μm. While the copper wire was used to make connection between pins of sample stage (Return (R) and Derive (D)) and $Ti_3C_2T_x$ free-standing MXene film as shown in schematic in Fig. 2(b).
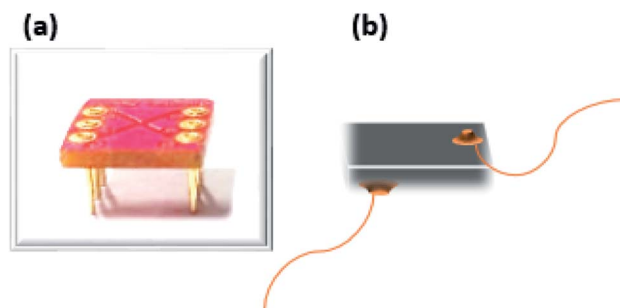

Fig. 2 (a) Sample stage, (b) $Ti_3C_2T_x$ free-standing MXene film with electrical connections.

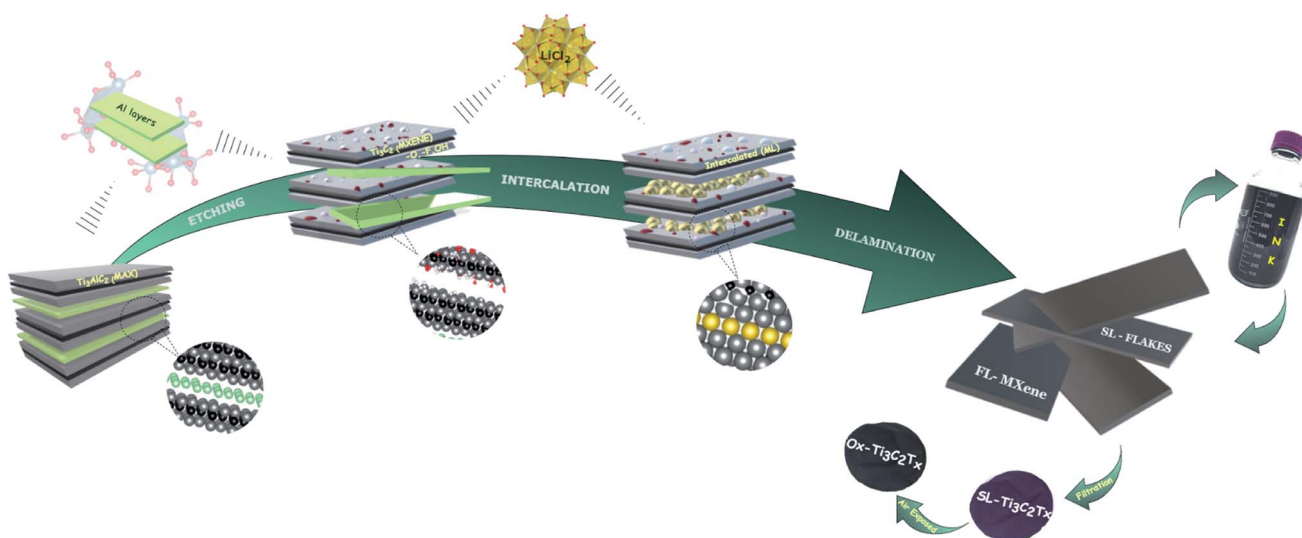Fig. 1 Synthesis scheme for production of de-laminated $Ti_3C_2T_x$ MXene film.

Result and discussion

Crystallographic studies of received MAX and synthesized MXene were carried out through X-ray diffraction (XRD) analysis (Fig. 3a). The XRD pattern of Ti_3AlC_2 MAX phase is in good agreement with the literature,[42] referring to JCPDS card# 52-0875. As can be seen from XRD pattern, our MAX phase is free of impurities. After the acidic etching and delamination, as expected, (00l) preferential symmetry of basal planes is observed in MXene flakes (indigo). All the peaks beyond $2\theta = 30°$ are absent in contrast to MAX phase. Also, the higher order (00l) peaks are of very weak intensity. A significant downshifting of (002) peak from $2\theta = 9.6°$ to $2\theta = 5.4°$ is a clear indication of complete exfoliation of MXene *via* removal of Aluminum layers.[44] This downshift towards a lower angle resulted in an increase in the *c*-lattice parameter from 18.4 Å of MAX to 32.8 Å in MXene and an increased *d*-spacing from 9.2 Å to 16.4 Å. The oxidation reflections are not visible in the XRD pattern which is due to the low fraction and smaller size of TiO_2 crystallites[45] however, the oxidation of MXene under room-temperature is a well-known phenomenon.[46,47] Fig. 3b exhibits the scanning electron micrograph (SEM) image of the bulk MAX phase while Fig. 3c is the cross-sectional image of delaminated $Ti_3C_2T_x$ MXene. The morphological image clearly suggests the successful formation of de-laminated MXene with well separated sheets.

Structural and phase transformations were studies through analysis of Raman spectra of the air exposed films heated at 100 °C and 300 °C (Fig. 4). The peaks present at 154 cm^{-1}, 409 cm^{-1} and 514 cm^{-1} are ascribed to TiO_2 anatase phase.[46,47] The peaks at 154 cm^{-1}, 260 cm^{-1} and 604 cm^{-1} confirm the presence of rutile phase.[48] Formation of anatase and rutile phases is due to the partial oxidation of $Ti_3C_2T_x$ MXene over the air exposure and heating effects. Moreover, a long time air exposure as well as heating at high temperature resulted in emergence of another phase, *i.e.* brookite phase of TiO_2. The peaks at 197 cm^{-1} and 409 cm^{-1} in ambient oxidized and 300 °C heat-treated systems are attributed to the brookite phase of TiO_2. These modes were not observed in the sample heated at
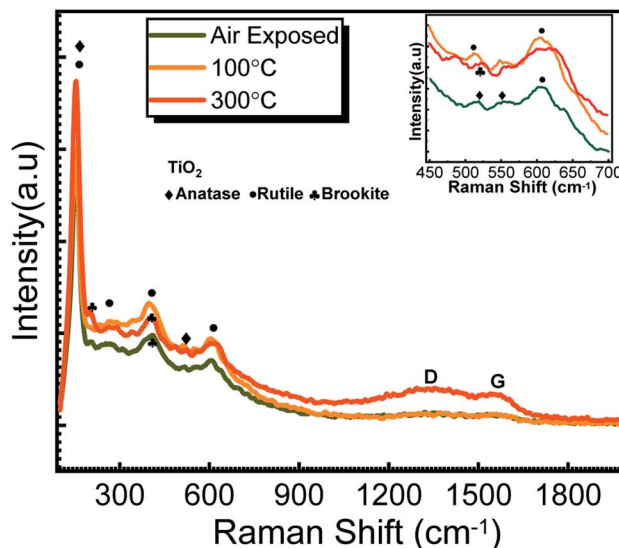
Fig. 4 Raman Spectra of oxidized air-exposed (dark green) and heat-treated samples at 100 °C (orange) and 300 °C $Ti_3C_2T_x$ MXene film.

relatively lower temperature (around 100 °C).[49–52] When heated at high temperature, two broader peaks at $\approx$1390 cm^{-1} and $\approx$1590 cm^{-1} are characterized as G and D bands of graphitic carbon. Broadening of D and G bands is an evidence of disordered or oxidized carbon, similar to what has been reported for graphene.[53] Presence of TiO_2 on the carbon sheets implies that the Ti atoms present in the inner MXene sheets have migrated to the top surface to react with oxygen leaving behind the defects. This kind of outward migration of Ti atoms is similar to the previous studies carried out on TiN.[54,55]

Fig. 5 presents unique ferroelectric, and multiferroic results of the heat-treated de-laminated free-standing $Ti_3C_2T_x$ MXene film. Fig. 5a shows spontaneous polarization *vs.* electric-field hysteresis loops for samples heated at 100 °C (left vertical column) and 150 °C (right vertical column) measured at room-temperature and frequency of 10 Hz that show clear ferroelectric hysteresis effect. As the electric-field is increased, the
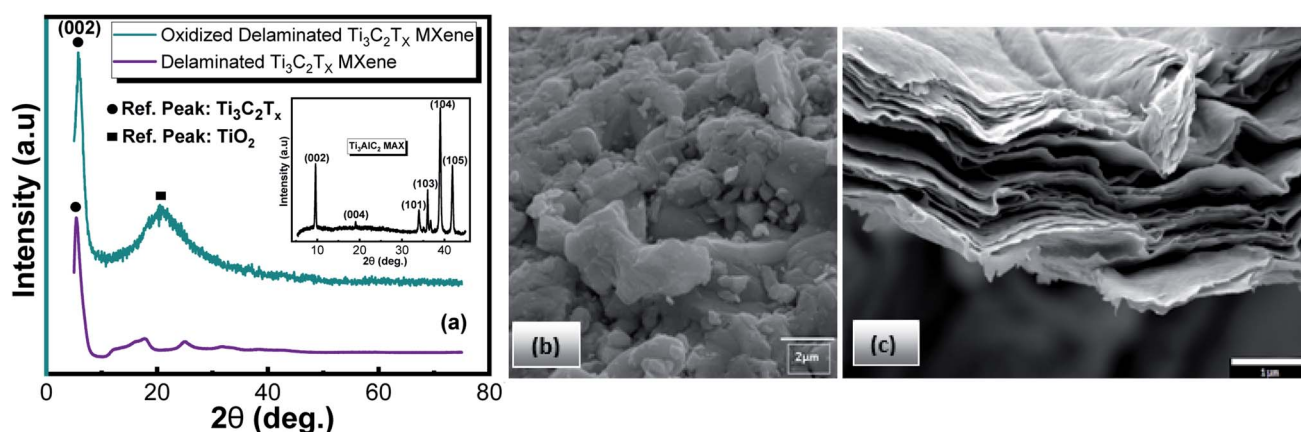
Fig. 3 (a) XRD pattern of $Ti_3C_2T_x$ MXene (purple) and heat-treated $Ti_3C_2T_x$ MXene film (green); inset: XRD of Ti_3AlC_2 MAX phase, (b) SEM micrographs of Ti_3AlC_2 MAX and (c) De-laminated $Ti_3C_2T_x$ MXene film.
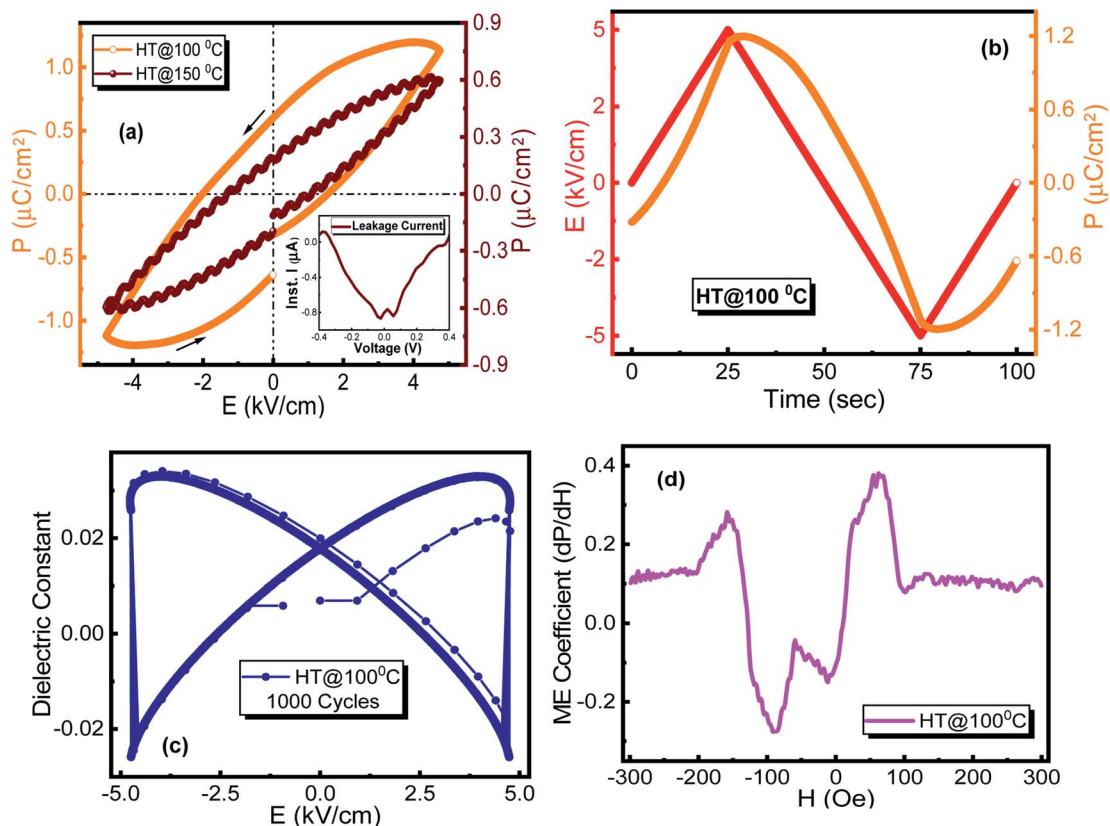
Fig. 5 (a) Ferroelectric hysteresis loops measured for heat-treated de-laminated $Ti_3C_2T_x$ MXene film at 100 °C (left vertical column) & 150 °C (right vertical column); inset shows typical leakage current *vs.* voltage that corresponds to the ferroelectric materials, (b) electric field (left vertical column) and electric polarization (right vertical column) *versus* time for heat-treated sample at 100 °C, (c) typical dielectric constant as a function of electric fields for heat-treated sample at 100 °C; the data is presented for 1000 cycles showing its reproducibility and stability, (d) the magnetoelectric coupling coefficient *versus* magnetic-field measured for heat-treated sample at 100 °C.

polarization increases as well due to alignment of the electric dipoles along the electric-field and reaches to the saturation value (maximum polarization) of 1 μC cm^{-2} and 0.6 μC cm^{-2} for HT@100 °C and HT@150 °C, respectively at +4 kV cm^{-1}. When the electric field is reduced to zero, the polarization falls to a non-zero remanant polarization value of 0.5 μC cm^{-2} and 0.28 μC cm^{-2} respectively for HT@100 °C and HT@150 °C which is a typical signature of hysteresis effect. It is important to note that the polarization–voltage measurements were also performed for air-exposed sample as well as the ones heated at temperatures higher than 150 °C (Fig. S1†) but the ferroelectric hysteresis effect was not observed. The polarization–voltage curve showed typical conductive behavior which either could be due to the under-formed or over-formed TiO_2 phase. This concludes that the induced ferroelectric effect remains stable for a narrow temperature range forming a suitable $TiO_2/Ti_3C_2T_x$ composite ratio. The inset of Fig. 5a shows current–voltage (*I–V*) measurements performed for HT@100 °C at room-temperature. The current is slightly asymmetric being higher for negative polarity and lower for positive polarity. The *I–V* results present a typical polarization-switching induced leakage current which is a characteristic of the ferroelectric material.[56,57] Fig. 5b represents electric field *versus* time (red) and polarization *versus* time (orange) measurements. The electric field follows linear

change with time in positive and negative polarity which polarizes the electric dipoles along positive and negative directions, respectively indicating fine tuning of the polarization. Also, the polarization curve at minimum (0 s) and maximum (100 s) time shows non-zero values which is due to the remanent effect. To the best of our knowledge, this is the first experimental report on existence of ferroelectricity in 2D MXene especially in the de-laminated free-standing film at room-temperature. One possibility for observation of this ferroelectricity in heat-treated MXene is the emergence of TiO_2 phase after heat treatment within $Ti_3C_2T_x$ MXene. Montanari *et al.*[58] performed density function calculations on rutile TiO_2 and concluded that it can show ferroelectricity under a uniaxial strain or a negative pressure. Yong Liu *et al.* also predicted a negative pressure induced ferroelectric phase in TiO_2.[25] A. Grunebohm *et al.* computationally studied the effect of strain which induced ferroelectricity in TiO_2 and concluded that even a non-uniaxial strain could induce a ferroelectric phase in TiO_2 where a small change in strain could produce a large spontaneous polarization.[27] The bond length between Ti–O is also reported to be a key parameter in determining proximity for inducing ferroelectricity where a small perturbation could drive the system ferroelectric.[59–61] Fig. 5c shows the butterfly-like dielectric constant-electric field hysteresis loops measured for

HT@100 °C at room-temperature. It is to be noted that the dielectric constant data is plotted for 1000 cycles that shows its high stability. The dielectric constant is initially small due to the small poling but increases at higher electric field and reaches the maximum at around the coercive field. At values closer to the saturation values of polarization, it reduces to its minimum value because all the dipoles get aligned and are unable to respond further to the increase in electric field.[62]

In order to observe the multiferroic effect in $Ti_3C_2T_x$ MXene film, the material must possess at least two ferroic orders (ferromagnetic, ferroelectric, *etc.*) simultaneously. In an earlier literature, Sunaina *et al.* reported the existence of ferromagnetism in $Ti_3C_2T_x$ MXene at room-temperature.[38] Since, our MXene showed a good ferroelectric response, it could show a multiferroic behavior as well because it was already reported to be a ferromagnet at room-temperature. The results presented in Fig. 5(a–c) clearly suggest that our heat-treated $Ti_3C_2T_x$ MXene film could behave like a multiferroic 2D material which can be confirmed by ME coupling effect.

Fig. 5d shows magnetoelectric results of heat-treated $Ti_3C_2T_x$ free-standing film measured at room-temperature using multiferroic/ferroelectric precision tester from Radiant Technologies Inc. The figure shows the magnetoelectric coupling coefficient *versus* applied magnetic field measured at room-temperature. The ME coefficient displays obvious peaks at specific magnetic field values which are close to the magnetic coercivity of the material itself. This suggests that the magnetic domains are strongly coupled with the electric domains which are well-tuned by the external magnetic field at room-temperature. Thus, our heat-treated $Ti_3C_2T_x$ film proved to possess strong multiferroic property due to the existence of ferroelectric as well as ferromagnetic orders. It is pertinent to mention that our report is the first experimental evidence on existence of multiferroicity in MXene, especially in the 2D de-laminated free-standing $Ti_3C_2T_x$ MXene film. Further studies on this effect in layered materials could enhance practical application scope of MXene in electric and magnetic data storage devices in the fields of spintronics and MXetronics.

Conclusion

We employed a simple approach to induce ferroelectricity and multiferroicity in free-standing heat-treated $Ti_3C_2T_x$ MXene film at room-temperature. The successful synthesized free-standing $Ti_3C_2T_x$ MXene, the films were heated at different temperatures produce TiO_2 layer on top of the $Ti_3C_2T_x$ MXene. Raman spectroscopy confirmed the presence of rutile and anatase phases of TiO_2. The composite film was tested for ferroelectric measurement that showed a clear hysteresis effect. The measured value of remanent polarization is 0.5 $\mu C\ cm^{-2}$. The effect was attributed to proximity-induced ferroelectricity in TiO_2 which was predicted before. Since, $Ti_3C_2T_x$ MXene film also reported to be a soft ferromagnet hence, we assumed that the composite film may also possess multiferroic property. To verify this assumption, the magnetoelectric (ME) testing was performed at room-temperature. Interestingly, the film showed a strong ME coupling with a good control of spontaneous polarization *via*

external magnetic field revealing the emergence of strong multiferroic effect as well. Our report is first experimental report on observation ferroelectric as well as multiferroic property in de-laminated heat-treated $Ti_3C_2T_x$ MXene film at room-temperature and presents MXene as the potential 2D material candidate for future data storage devices.

Data availability

The data will be available on demand.

Author contributions

Rabia Tahir performed testing and analysis of results, Syedah Afsheen Zahra prepared MXene paper, Usman Naeem helped in sample preparation, Deji Akinwande helped in analysis of results and Syed Rizwan conceived the idea, performed the measurement and analysis.

Conflicts of interest

There are no conflicts to declare.

Acknowledgements

References

1 S.-W. Cheong and M. Mostovoy, Multiferroics: a magnetic twist for ferroelectricity, *Nat. Mater.*, 2007, **6**(1), 13–20.

2 S. Rizwan, S. Zhang, Y. G. Zhao and X. F. Han, Exchange-bias like hysteretic magnetoelectric-coupling of as-grown synthetic antiferromagnetic structures, *Appl. Phys. Lett.*, 2012, **101**(8), 082414.

3 S. Rizwan, G. Q. Yu, S. Zhang, Y. G. Zhao and X. F. Han, Electric-field control of CoFeB/IrMn exchange bias system, *J. Appl. Phys.*, 2012, **112**(6), 064120.

4 N. A. Spaldin and R. Ramesh, Advances in magnetoelectric multiferroics, *Nat. Mater.*, 2019, **18**(3), 203–212.

5 C. Lu, W. Hu, Y. Tian and T. Wu, Multiferroic oxide thin films and heterostructures, *Appl. Phys. Rev.*, 2015, **2**(2), 021304.

6 A. Chandrasekaran, A. Mishra and A. K. Singh, Ferroelectricity, antiferroelectricity, and ultrathin 2D electron/hole gas in multifunctional monolayer MXene, *Nano Lett.*, 2017, **17**(5), 3290–3296.

7 D. Wijethunge, L. Zhang and A. Du, Prediction of two-dimensional ferroelectric metal Mxenes, *J. Mater. Chem. C*, 2021, **9**(34), 11343–11348.

8 Ki C. Kwon, Y. Zhang, L. Wang, W. Yu, X. Wang, I.-H. Park, H. S. Choi, et al. In-plane ferroelectric tin monosulfide and its application in a ferroelectric analog synaptic device, *ACS Nano*, 2020, **14**(6), 7628–7638.

9 H. Wang, W. Lu, S. Hou, B. Yu, Z. Zhou, Y. Xue, R. Guo, S. Wang, K. Zeng and X. Yan, A 2D-SnSe film with ferroelectricity and its bio-realistic synapse application, *Nanoscale*, 2020, **12**(42), 21913–21922.

10 S. Yuan, X. Luo, H. L. Chan, C. Xiao, Y. Dai, M. Xie and J. Hao, Room-temperature ferroelectricity in MoTe$_2$ down to the atomic monolayer limit, *Nat. Commun.*, 2019, **10**(1), 1–6.

11 Z. Fei, W. Zhao, T. A. Palomaki, B. Sun, M. K. Miller, Z. Zhao, J. Yan, X. Xu and D. H. Cobden, Ferroelectric switching of a two-dimensional metal, *Nature*, 2018, **560**(7718), 336–339.

12 L. You, F. Liu, H. Li, Y. Hu, S. Zhou, L. Chang, Y. Zhou, et al. In-Plane Ferroelectricity in Thin Flakes of Van der Waals Hybrid Perovskite, *Adv. Mater.*, 2018, **30**, 1803249.

13 F. Xue, W. Hu, Ko-C. Lee, Li-S. Lu, J. Zhang, H. -L. Tang, A. Han, et al. Room-temperature ferroelectricity in hexagonally layered α-In$_2$Se$_3$ nanoflakes down to the monolayer limit, *Adv. Funct. Mater.*, 2018, **28**, 1803738.

14 C. Zheng, Y. Lei, L. Zhu, J. L. Collins, D. Kim, Y. Lou, C. Xu, et al. Room temperature in-plane ferroelectricity in van der Waals In$_2$Se$_3$, *Sci. Adv.*, 2018, **4**(7), eaar7720.

15 J. Xiao, H. Zhu, Y. Wang, W. Feng, Y. Hu, A. Dasgupta, Y. Han, et al. Intrinsic two-dimensional ferroelectricity with dipole locking, *Phys. Rev. Lett.*, 2018, **120**(22), 227601.

16 Y. Zhou, D. Wu, Y. Zhu, Y. Cho, Q. He, X. Yang, K. Herrera, et al. Out-of-plane piezoelectricity and ferroelectricity in layered α-In$_2$Se$_3$ nanoflakes, *Nano Lett.*, 2017, **17**(9), 5508–5513.

17 K. Chang, J. Liu, H. Lin, N. Wang, K. Zhao, A. Zhang, F. Jin, et al. Discovery of robust in-plane ferroelectricity in atomic-thick SnTe, *Science*, 2016, **353**(6296), 274–278.

18 A. Belianinov, H. Qian, A. Dziaugys, P. Maksymovych, E. Eliseev, A. Borisevich, A. Morozovska, J. Banys, Y. Vysochanskii and S. V. Kalinin, CuInP$_2$S$_6$ room temperature layered ferroelectric, *Nano Lett.*, 2015, **15**(6), 3808–3814.

19 J.-J. Zhang, L. Lin, Y. Zhang, M. Wu, B. I. Yakobson and S. Dong, Type-II multiferroic Hf$_2$VC$_2$F$_2$ MXene monolayer with high transition temperature, *J. Am. Chem. Soc.*, 2018, **140**(30), 9768–9773.

20 M. Wu and X. C. Zeng, Intrinsic ferroelasticity and/or multiferroicity in two-dimensional phosphorene and phosphorene analogues, *Nano Lett.*, 2016, **16**(5), 3236–3241.

21 H. Ju, Y. Lee, K.-T. Kim, In H. Choi, J. R. Chang, S. Son, P. Park, et al. Possible persistence of multiferroic order down to bilayer limit of van der Waals material NiI$_2$, *Nano Lett.*, 2021, **21**(12), 5126–5132.

22 H. Qiao, C. Wang, W. S. Choi, M. H. Park and Y. Kim, Ultra-thin ferroelectrics, *Mater. Sci. Eng., R*, 2021, **145**, 100622.

23 A. Lipatov, P. Chaudhary, Z. Guan, H. Lu, G. Li, C. Olivier, K. Dodzi Dorkenoo, et al. Direct observation of ferroelectricity in two-dimensional MoS$_2$, *npj 2D Mater. Appl.*, 2022, **6**(1), 1–9.

24 Y. Yu, L.-D. Wang, W.-L. Li, Y.-L. Qiao, Y. Zhao, F. Yu, T.-D. Zhang, R.-X. Song and W.-D. Fei, Room temperature ferroelectricity in donor-acceptor co-doped TiO$_2$ ceramics using doping-engineering, *Acta Mater.*, 2018, **150**, 173–181.

25 Y. Liu, L. Ni, Z. Ren, G. Xu, C. Song and G. Han, Negative pressure induced ferroelectric phase transition in rutile TiO$_2$, *J. Phys.: Condens. Matter*, 2009, **21**(27), 275901.

26 Y. Yu, L.-D. Wang, W.-L. Li, Y.-L. Qiao, Y. Zhao, F. Yu, T.-D. Zhang, R.-X. Song and W.-D. Fei, Room temperature ferroelectricity in donor-acceptor co-doped TiO$_2$ ceramics using doping-engineering, *Acta Mater.*, 2018, **150**, 173–181.

27 A. Grünebohm, C. Ederer and P. Entel, First-principles study of the influence of (110)-oriented strain on the ferroelectric properties of rutile TiO$_2$, *Phys. Rev. B*, 2011, **84**(13), 132105.

28 J. Halim, M. R. Lukatskaya, K. M. Cook, J. Lu, C. R. Smith, L.-Å. Näslund, S. J. May, et al. Transparent conductive two-dimensional titanium carbide epitaxial thin films, *Chem. Mater.*, 2014, **26**(7), 2374–2381.

29 M. Mariano, O. Mashtalir, F. Q. Antonio, W.-H. Ryu, B. Deng, F. Xia, Y. Gogotsi and A. D. Taylor, Solution-processed titanium carbide MXene films examined as highly transparent conductors, *Nanoscale*, 2016, **8**(36), 16371–16378.

30 S. Lai, J. Jeon, S. K. Jang, J. Xu, Y. J. Choi, J.-H. Park, E. Hwang and S. Lee, Surface group modification and carrier transport properties of layered transition metal carbides (Ti$_2$CT$_x$, T:–OH,–F and–O), *Nanoscale*, 2015, **7**(46), 19390–19396.

31 M. R. Lukatskaya, O. Mashtalir, C. E. Ren, Y. Dall'Agnese, P. Rozier, P. L. Taberna, M. Naguib, P. Simon, M. W. Barsoum and Y. Gogotsi, Cation intercalation and high volumetric capacitance of two-dimensional titanium carbide, *Science*, 2013, **341**(6153), 1502–1505.

32 M. Ghidiu, M. R. Lukatskaya, M.-Q. Zhao, Y. Gogotsi and M. W. Barsoum, Conductive two-dimensional titanium carbide 'clay' with high volumetric capacitance, *Nature*, 2014, **516**(7529), 78–81.

33 Y. Yang, S. Umrao, L. Shen and S. Lee, Large-area highly conductive transparent two-dimensional Ti$_2$CT$_x$ film, *J. Phys. Chem. Lett.*, 2017, **8**(4), 859–865.

34 M. Naguib, J. Halim, J. Lu, K. M. Cook, L. Hultman, Y. Gogotsi and M. W. Barsoum, New two-dimensional niobium and vanadium carbides as promising materials for Li-ion batteries, *J. Am. Chem. Soc.*, 2013, **135**(43), 15966–15969.

35 R. B. Rakhi, B. Ahmed, M. N. Hedhili, D. H. Anjum and H. N. Alshareef, Effect of postetch annealing gas composition on the structural and electrochemical properties of Ti$_2$CT$_x$ MXene electrodes for supercapacitor applications, *Chem. Mater.*, 2015, **27**(15), 5314–5323.

36 Y. Xie, Y. Dall'Agnese, M. Naguib, Y. Gogotsi, M. W. Barsoum, H. L. Zhuang and P. R. C. Kent, Prediction and characterization of MXene nanosheet anodes for non-lithium-ion batteries, *ACS Nano*, 2014, **8**(9), 9606–9615.

37 F. Liu, A. Zhou, J. Chen, H. Zhang, J. Cao, L. Wang and Q. Hu, Preparation and methane adsorption of two-dimensional carbide Ti$_2$C, *Adsorption*, 2016, **22**(7), 915–922.

38 S. Rafiq, S. U. Awan, R.-K. Zheng, Z. Wen, M. Rani, D. Akinwande and R. Syed, Novel room-temperature ferromagnetism in Gd-doped 2-dimensional Ti$_3$C$_2$T$_x$

MXene semiconductor for spintronics, *J. Magn. Magn. Mater.*, 2020, **497**, 165954.

39 M. Iqbal, J. Fatheema, Q. Noor, M. Rani, M. Mumtaz, R.-K. Zheng, S. A. Khan and R. Syed, Co-existence of magnetic phases in two-dimensional MXene, *Mater. Today Chem.*, 2020, **16**, 100271.

40 Z. U. D. Babar, M. S. Anwar, M. Mumtaz, M. Iqbal, R.-K. Zheng, D. Akinwande and R. Syed, Peculiar magnetic behaviour and Meissner effect in two-dimensional layered Nb$_2$C MXene, *2D Materials*, 2020, **7**(3), 035012.

41 J. Low, L. Zhang, T. Tong, B. Shen and J. Yu, TiO$_2$/MXene Ti$_3$C$_2$ composite with excellent photocatalytic CO$_2$ reduction activity, *J. Catal.*, 2018, **361**, 255–266.

42 J. Luo, W. Zhang, H. Yuan, C. Jin, L. Zhang, H. Huang, C. Liang, et al. Pillared structure design of MXene with ultralarge interlayer spacing for high-performance lithium-ion capacitors, *ACS Nano*, 2017, **11**(3), 2459–2469.

43 L. Zhang, C. Tang, C. Zhang and A. Du, First-principles screening of novel ferroelectric MXene phases with a large piezoelectric response and unusual auxeticity, *Nanoscale*, 2020, **12**(41), 21291–21298.

44 A. Lipatov, A. Mohamed, M. R. Lukatskaya, A. Boson, Y. Gogotsi and S. Alexander, Effect of synthesis on quality, electronic properties and environmental stability of individual monolayer Ti$_3$C$_2$ MXene flakes, *Adv. Electron. Mater.*, 2016, **2**(12), 1600255.

45 S. Chertopalov and V. N. Mochalin, Environment-sensitive photoresponse of spontaneously partially oxidized Ti$_3$C$_2$ MXene thin films, *ACS Nano*, 2018, **12**(6), 6109–6116.

46 M. Cao, F. Wang, L. Wang, W. Wu, W. Lv and J. Zhu, Room temperature oxidation of Ti$_3$C$_2$ MXene for supercapacitor electrodes, *J. Electrochem. Soc.*, 2017, **164**(14), A3933.

47 C. J. Zhang, S. Pinilla, N. McEvoy, C. P. Cullen, B. Anasori, E. Long, S.-H. Park, et al. Oxidation stability of colloidal two-dimensional titanium carbides (MXenes), *Chem. Mater.*, 2017, **29**(11), 4848–4856.

48 X. Li, X. Yin, M. Han, C. Song, H. Xu, Z. Hou, L. Zhang and L. Cheng, Ti$_3$C$_2$ MXenes modified with in situ grown carbon nanotubes for enhanced electromagnetic wave absorption properties, *J. Mater. Chem. C*, 2017, **5**(16), 4068–4074.

49 J. Chen, M. Guan, X. Zhang and X. Gong, Insights into a rutile/brookite homojunction of titanium dioxide: Separated reactive sites and boosted photocatalytic activity, *RSC Adv.*, 2019, **9**, 36615–36620.

50 G. A. Tompsett, G. A. Bowmaker, R. P. Cooney, J. B. Metson, K. A. Rodgers and J. M. Seakins, The Raman spectrum of brookite, TiO$_2$ (Pbca, Z = 8), *J. Raman Spectrosc.*, 1995, **26**, 57–62.

51 R. Verma, J. Gangwar and A. K. Srivastava, Multiphase TiO$_2$ nanostructures: A review of efficient synthesis, growth mechanism, probing capabilities, and applications in bio-safety and health, *RSC Adv.*, 2017, **7**(70), 44199–44224.

52 M. C. Ceballos-Chuc, C. M. Ramos-Castillo, J. J. Alvarado-Gil, G. Oskam and G. Rodríguez-Gattorno, Influence of brookite impurities on the Raman spectrum of TiO$_2$ anatase nanocrystals, *J. Phys. Chem. C*, 2018, **122**, 19921–19930.

53 Y. Yoon, T. A. Le, A. P. Tiwari, I. Kim, M. W. Barsoum and H. Lee, Low temperature solution synthesis of reduced two dimensional Ti$_3$C$_2$ MXenes with paramagnetic behaviour, *Nanoscale*, 2018, **10**, 22429–22438.

54 Yu G. Gogotsi and F. Porz, The oxidation of particulate-reinforced Si$_3$N$_4$-TiN composites, *Corros. Sci.*, 1992, **33**(4), 627–640.

55 N. Michael, O. Mashtalir, M. R. Lukatskaya, B. Dyatkin, C. Zhang, V. Presser, Y. Gogotsi and M. W. Barsoum, One-step synthesis of nanocrystalline transition metal oxides on thin sheets of disordered graphitic carbon by oxidation of MXenes, *Chem. Commun.*, 2014, **50**(56), 7420–7423.

56 L. Pintilie, I. Vrejoiu, D. Hesse, G. LeRhun and M. Alexe, Ferroelectric polarization-leakage current in high quality epitaxial Pb(Zr, Ti)O$_3$ films, *Phys. Rev. B: Condens. Matter Mater. Phys.*, 2007, **75**, 104103.

57 A. G. Boni, C. Chirila, L. Hrib, I. Pintilie and L. Pintilie, Study of the leakage current in epitaxial ferroelectric Pb(Zr$_{0.52}$Ti$_{0.48}$)O$_3$ layer with SrRuO$_3$ bottom electrode and different metals as top contacts, *Dig. J. Nanomater. Biostructures*, 2015, **10**, 1257.

58 B. Montanari and N. M. Harrison, Pressure-induced instabilities in bulk TiO$_2$ rutile, *J. Phys.: Condens. Matter*, 2004, **16**(3), 273.

59 J. H. Barrett, Dielectric constant in perovskite type crystals, *Phys. Rev.*, 1952, **86**(1), 118.

60 C. Ang, Z. Yu, P. M. Vilarinho and J. L. Baptista, B i: SrTiO$_3$: A quantum ferroelectric and a relaxor, *Phys. Rev. B: Condens. Matter Mater. Phys.*, 1998, **57**(13), 7403.

61 T. Mitsui and W. Blackburn Westphal, Dielectric and X-Ray Studies of Ca$_x$Ba $_{1-x}$Ti$_3$ and Ca$_x$Sr$_{1-x}$TiO$_3$, *Phys. Rev.*, 1961, **124**(5), 1354.

62 S. J. Kim, J. Mohan, C. D Young, L. Colombo, J Kim, S. R. Summerfelt and T. San, Ferroelectric TiN/Hf$_{0.5}$Zr$_{0.5}$O$_2$/TiN capacitors with low-voltage operation and high reliability for next-generation FRAM applications, *IEEE*, 2018, **18**, 5386.